Available online at www.sciencedirect.com
SCIENCE DIRECT
Polymer 46 (2005) 9314–9328
polymer
www.elsevier.com/locate/polymer

Preparation and flame resistance properties of revolutionary self-extinguishing epoxy nanocomposites based on layered double hydroxides

Mauro Zammarano[a,*,1], Massimiliano Franceschi[b], Séverine Bellayer[a,2], Jeffrey W. Gilman[a], Sergio Meriani[c]

[a]*Building and Fire Research Laboratory, National Institute of Standards and Technology, 100 Bureau Drive, Gaithersburg, MD 20899-8665, USA*
[b]*Cimteclab, Area Science Park, Padriciano 99, 34012 Trieste, Italy*
[c]*Materials and Natural Resources Department, University of Trieste, Valerio 2, 34127 Trieste, Italy*

Received 15 March 2005; received in revised form 5 July 2005; accepted 14 July 2005
Available online 10 August 2005

Abstract

Layered double hydroxides/epoxy (LDHs/EP) nanocomposites were prepared from organo-modified LDHs, a diglycidyl ether of bisphenol A monomer (DGEBA) and amine curing agents. The organo-modified LDHs were obtained by ionic exchange of a magnesium–aluminum carbonate LDH in an acid medium. X-ray diffraction and transmission electron microscopy showed a dispersion of the layers at a nanometer scale, indicating the formation of LDH/EP nanocomposites. The thermal degradation and flame resistance properties of LDH/EP nanocomposites, montmorillonite–epoxy (MMT/EP) nanocomposites, LDH/EP microcomposites and aluminum hydroxide–epoxy microcomposites were compared by thermogravimetrical analyses, simultaneous thermal analyses, UL94 and cone calorimeter tests. Only LDH/EP nanocomposites showed self-extinguishing behavior in the horizontal UL94 test; LDH/EP microcomposites and MMT/EP nanocomposites samples burned completely showing that the unique flame resistance of LDH/EP nanocomposites is related to both the level of dispersion and the intrinsic properties of LDH clay. Furthermore, cone calorimeter revealed intumescent behavior for LDH/EP nanocomposites and a higher reduction in the peak heat release rate compared to MMT/EP nanocomposites.

Keywords: Epoxy; Nanocomposite; LDH

1. Introduction

The aim of the present work concerns the use of layered double hydroxides (LDHs), as an alternative to commonly used cationic clays, to formulate epoxy nanocomposites with high flame retardant properties. LDHs are a family of layered crystals [1] that have an octahedral structure similar to brucite—$Mg(OH)_2$—where the partial isomorphous replacement of a bivalent cation with a trivalent cation produces positive charges counter balanced by hydrated anions. By analogy with some lamellar cationic clays such as 2:1 phyllosilicates, the minerals belonging to the group of LDHs are called anionic clays. Like cationic clays, LDHs can be modified by intercalating organic ions between the lamellas and can be profitably used as nanofillers for the synthesis of nanocomposites [2]. It is reported that LDHs contribute to the flame retardancy of the polymeric matrix, producing a refractory oxide residue on the surface of the material and releasing aqueous vapour and carbon dioxide during the decomposition. The endothermic nature of these processes and the dilution of combustible gases of pyrolysis increase the ignition time and reduce the heat release during the combustion [3].

In this study the flame retardant effectiveness of nanodispersed LDH in epoxy resin is compared with nanodispersed montmorillonite clay and conventional

* Corresponding author. Tel.: +39 064 52215283; fax: +39 08318331185.
E-mail address: zammarano@gmail.com (M. Zammarano).
[1] NIST Guest Researcher from CimtecLab, Area Science Park, Padriciano 99, 34012 Trieste, Italy.
[2] NIST Guest Researcher from Laboratory GEMTEX of Ecole Nationale Supérieure des Arts et Industries Textiles (ENSAIT).

0032-3861/$ - see front matter © 2005 Elsevier Ltd. All rights reserved.
doi:10.1016/j.polymer.2005.07.050

microfillers such as aluminium trihydroxide and ammonium polyphosphate. A unique self-extinguishing behavior of LDH/epoxy nanocomposites was observed in UL94HB with 5 wt%[3] of organo-modified anionic clays. The effectiveness of these systems was confirmed by cone calorimetry. Furthermore, a synergistic effect between ammonium polyphosphate and LDH was observed with UL94-VB (vertical burning) test.

2. Experimental[4]

2.1. Materials

The organo-modified anionic clays were prepared by ionic exchange of a synthetic magnesium–aluminum carbonate LDH precursor-PURAL MG61HT—kindly supplied from Sasol Germany GmbH. Three different types of organic acids were used to increase the surface hydrophobicity of pristine LDH, 3-aminobenzenesulfonic acid (ABS) (Fluka, assay ≥ 98%), 4-toluenesulfonic acid monohydrate (TS) (Aldrich, assay ≥ 98.5%) and 4-hydroxybenzenesulfonic acid (HBS) (Aldrich, 65% wt in water). A montmorillonite modified with C14–C18 primary alkylamine—Dellite AP (DelAP)—was supplied from Laviosa Chimica Mineraria (Livorno, Italy) and a quaternary ammonium salt modified montmorillonite-Cloisite 30B (30B)—was supplied from Southern Clay Products. Aluminum trihydroxide—Apyral 40 (ATH)—from Nabaltec, and ammonium polyphosphate—EXOLIT AP422 $(NH_4PO_3)_n$ $n = 700$ (APP)—from Clariant, were used for reference as microfillers. A diglycidyl ether of bisphenol A epoxy monomer—DER331—was obtained from Dow Plastics. Triethylene tetra amine (DEH 24, Dow Plastics), 4,4′-diaminodiphenyl sulfone (DDS, Aldrich) and poly(propylene glycol)bis(2-aminopropyl) ether (Jeffamine D230, Huntsman Corp.) were used as curing agents. The chemical structures of the different reagents are presented in Fig. 1.

2.2. Synthesis of the organo-modified LDHs

The pristine magnesium–aluminium LDH MG61HT with a mole ratio Mg:Al = 2:1 is modified by ionic exchange in a acid medium. For the remainder of this publication the identification names MG61, MG61/ABS, MG61/TS and

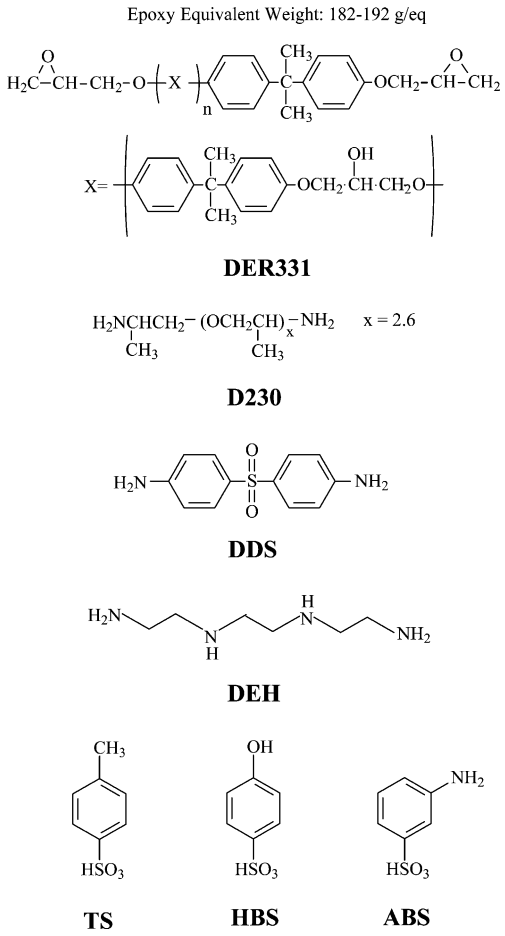

Fig. 1. Chemical structures of the epoxy monomer DER331; curing agents D230, DDS, DEH; organic modifiers TS, HBS, ABS.

Table 1
Description and sample identification of anionic clays

Sample ID	Organic modifier	Anion size[a] (nm)	$d_{calculated}$[b] (nm)	$d_{experimental}$ (nm)
MG61	–	–	–	0.76
MG61/ABS[c]	3-Amino-benzenesul-fonate	0.85	1.64	1.59
MG61/TS	4-Toluene-sulfonate	0.93	1.72	1.71
MG61/HBS	4-Hydroxy-benzenesul-fonate	0.90	1.69	1.52

[a] Estimated value obtained assuming that van der Waals radius of O is 0.13 nm and of H is 0.11 nm; anion is oriented with long axis perpendicular to hydroxyl layers.

[b] $d_{calculated} = d_{layer} + d_{anion} + d_{water}$, where $d_{layer} = 0.48$ nm is the thickness of brucite-type layer [4] and $d_{water} = 0.31$ nm is the adsorbed water molecule size on the hydroxyl layer.

[c] MG61/ABSair and MG61/ABSsx are similar to MG61/ABS but they are washed and dried, respectively, in air and Soxhlet extractor instead of N_2.

[3] Weight percentage means mass fraction% and is used as such through out this manuscript.

[4] This work was carried out by the National Institute of Standards and Technology (NIST), an agency of the US government and by statue is not subject to copyright in USA. The identification of any commercial product or trade name does not imply endorsement or recommendation by NIST. The policy of NIST is to use metric units of measurement in all its publications, and to provide statements of uncertainty for all original measurements. In this document, however, data from organizations outside NIST are shown, which may include measurements in non-metric units or measurements without uncertainty statements.

MG61/HBS (provided in Table 1) will refer to the pristine LDH precursor and the modified LDH with ABS, TS and HBS, respectively. For the synthesis of MG61/ABS, MG61 (36.0 g) was dispersed in distilled water (1800 mL) and ABS (64.8 g, 374.1 mmol) was dispersed in the mixture by stirring at 100 rad/s at 50 °C for 2 h. An excess of ABS was used (i.e. mole ratio ABS:Al = 2.4:1). The resulting slurry was filtered in a nitrogen atmosphere, washed first with decarbonated water and then a small amount of ethanol[5]. The product was dried in vacuo at 50 °C. The same procedure was used for the synthesis of MG61/TS and MG61/HBS but in these cases MG61 (10.0 g) was dispersed in distilled water (500 mL), and TS (14.4 g, mole ratio TS:Al = 1.78) or HBS (8.55 g, mole ratio TS:Al = 1.15), respectively, was dissolved in the mixture. For MG61/ABS an alternative method was used in which the slurry was quickly filtered without washing and dried in vacuo at 100 °C; the obtained material was ground, Soxhlet extracted (12 h) with boiling water (reflux) and argon atmosphere, and finally dried again in vacuo at 100 °C overnight. This sample will be identified as MG61/ABSsx.

2.3. Preparation of epoxy micro/nano-composites

The swelling of organic modified clays was achieved by hot stirring with the epoxy resin. For the samples cured with D230 the swelling conditions were 12 h at 80 °C and 2 h at 120 °C, and the curing conditions 5 h at 50 °C and 2 h at 110 °C. For the samples cured with DEH and DDS the anionic clay was first dispersed in *n*-butanol for 1 h by sonication, stirred with epoxy at 130 °C for 2 h, and finally heated in vacuo at 145 °C for 2 h to allow the evaporation of *n*-butanol. The samples were cured with DEH (17 h at room temperature, 1 h at 70 °C and 2 h at 120 °C) or DDS (2 h at 150 °C and 2 h at 175 °C). The samples containing the microfillers ATH and APP were dispersed by stirring at 50 °C for 10 min and were cured with the previous described conditions, which varied depending on the curing agent. The concentration of micro/nano-filler was 5 wt%. Before curing all samples were degassed and a stoichiometric amount of hardener was used. When the preparation of an epoxy sample cured by DDS containing APP was attempted (APP-DDS), the low viscosity of the mixture, at the curing temperature, allowed a complete settling of APP was observed. Instead a stable mixture was obtained for ABSsx-DDS nanocomposite. A comprehensive description of sample preparations and identification names is reported in Table 2.

2.4. Characterizations and measurements

The X-ray diffraction (XRD) was performed using a Bruker electronic instruments D5005 equipped with a Cu K_α tube ($\lambda = 0.15418$ nm) with θ–2θ geometry, step size 0.02°, step time 4 s for epoxy nanocomposites and 2 s for clays, *d*-spacing uncertainty of 0.01 nm (2σ) as determined by running a modified LDH (MG61/ABS) several times. For X-ray diffraction on liquid samples (LXRD), to allow the analysis of the fluid in a fixed horizontal position, a Bruker D8 system with θ–θ geometry was used, step size 0.02°, step time 4 s, Cu K_α tube. Carbon, hydrogen, nitrogen, sulfur, aluminum, magnesium, chlorine and water content of MG61/ABS were determined by Galbraith Laboratories, Inc. (Knoxville, TN, USA). The transmission electron microscopy (TEM) images were obtained on a Philips EM 208 with an acceleration voltage of 120 kV. The solid samples were ultramicromed with a diamond knife on Leica Ultracut UCT microtome to give 70 nm thick sections. For liquid samples, a thin layer of fluid was directly spread on a grid for TEM observation. The thermogravimetric analysis (TGA) was performed on a Hi Res TGA 2950 TA instrument with platinum pans; the size of the samples was about 10 mg, the heating rate 10 °C/min in nitrogen atmosphere (flowing rate 50 mL/min), and the peak mass loss rate had an uncertainty of 1.5 °C.

Simultaneous thermal analysis (STA) was performed on Netzsch STA 409 in air flow (75 mL/min) with a heating rate of 10 °C/min, sample size of 20 mg, typical uncertainty 1.9 °C in peak decomposition temperature. The differential scanning calorimetry (DSC) was recorded using a Perkin–Elmer Pyris 1; the scanning rate was 10 °C/min, the nitrogen

Table 2
Description and sample identification of epoxy micro/nano-composites

Sample ID	Filler[a]	Curing agent	Preparation	*d*-spacing (nm)
D230	–	D230	A	–
MG61-D230	MG61	D230	B	0.8
ABS-D230	MG61/ABS	D230	A	5.6
TS-D230	MG61/TS	D230	A	2.3
HBS-D230	MG61/HBS	D230	A	–
DAP-D230	DelAP	D230	A	7.0
30B-D230	30B	D230	A	4.0
APP-D230	APP	D230	B	–
ATH-D230	ATH	D230	B	–
DEH	–	DEH	C/BuOH	–
ABSsx-DEH	MG61/ABSsx	DEH	C/BuOH	3.3
APP-DEH	APP	DEH	C/BuOH	–
DDS	–	DDS	D/BuOH	–
ABSsx-DDS	MG61/ABSsx	DDS	D/BuOH	3.4
APP-DDS[b]	APP	DDS	D/BuOH	–

A, swelled for 12 h at 80 °C and 2 h at 120 °C—cured for 5 h at 50 °C and 2 h at 110 °C; B, hot stirred for 10 min at 50 °C—cured for 5 h at 50 °C and 2 h at 110 °C; C, swelled for 2 h at 130 °C—heated in vacuo for 2 h at 145 °C—cured for 17 h at RT, 1 h at 70 °C and 2 h at 120 °C; D, swelled 2 h 130 °C—heated in vacuo 2 h 145 °C—cured 2 h 150 °C, 2 h 175 °C; BuOH, swelled or mixed with *n*-butanol.

[a] The filler content is 5 wt% for all samples.

[b] A complete settling of APP was observed during curing.

[5] Ethanol was used in order to remove most of the water and reduce carbonate contamination during following handling and drying.

flowing rate 50 mL/min, the sample size around 10 mg and the glass transition temperature uncertainty 2 °C. Infrared spectra were collected using a Thermo Nicolet Nexus spectrophotometer equipped with an attenuated total reflectance (ATR) device—SensIR Technologies Durascope. Data were collected using 128 scans per spectra at a resolution of 4 cm^{-1}.

Evaluations of flammability were achieved using the cone calorimeter [5] and UL94 [6] tests. For the cone calorimeter test, the mixtures were cured in aluminum square molds (100×100 mm^2). The cone data reported here are obtained at 35 kW/m^2 and are the average of two or three replicated samples. The peak heat release rate, mass loss rate, and specific extinction area data are reproducible to within $\pm 10\%$; the heat of combustion and the time to ignition data are reproducible to within $\pm 15\%$.

Standard bar specimens—125 mm long by 13 mm wide and 3.2 mm thick—were prepared pouring the mixtures in a Teflon mold. Three specimens were tested for each composition in UL94 Horizontal Burning and one or two sets of five specimens were used for UL94 Vertical Burning. The linear burning rate data reported here are the averages of three samples and have an uncertainty of 2 mm/min. In order to estimate the van der Waals dimensions of intercalated species, SymApps software (Bio-Rad Laboratories) with a molecular mechanics based on the MM2 force field, was used.

3. Results and discussion

3.1. General characterization

The Mg/Al LDH—MG61—is the precursor used for the preparation of organo-modified LDHs; its chemical formula for octahedral unit is:

$$Mg_{(1-x)}Al_x(OH)_2\left(CO_3^{2-}\right)_{x/2}\cdot nH_2O \quad (1)$$

where $x = 0.333$ and $n \sim 0.5$

The molecular weight is $M_w = 78.23$ g/mol[6], the theoretical anionic exchange capacity (AEC) is 425 mequiv/100 g[7] and the layer charge density (σ) is 4.12 charge/nm^2 [8]. For comparison, a sodium montmorillonite cationic clay, with a medium value of exchange capacity (108 mequiv/100 g), has a value of $\sigma = 1.43$ charge/nm^2 [2]. The high charge density of anionic clays generates strong electrostatic forces between the layers and the anions, thus, swelling and exfoliation process are much more difficult [7–9]. This may explain the relatively low number of LDH based nanocomposites reported in literature. Another drawback for LDHs is their high affinity for carbonate anion, due to its high anion charge density [10]. The anion selectivity increases with increasing anion charge density [11], i.e. anionic clays strongly prefer multiply charged anions. Thus synthesis and anionic exchange must be completed in an inert atmosphere in order to avoid contamination from CO_2. MG61 (Eq. (1)) is a LDH in a carbonate form, i.e. the intercalated anion is carbonate. In spite of this, the carbonate anions were successfully exchanged in an acid medium with monovalent organic anions, because, at low pH values, carbonate anions are neutralized and released as CO_2. For the synthesis of organo-modified LDH, the amount of organic acids was adjusted to obtain a final pH ~ 4. The influence of pH on intercalation was observed also in previous works [12]. The shift of the *d*-spacing d_{003} from 0.76 nm in the MG61 (Fig. 2) to higher values (Fig. 3) suggests the evidence of the replacement of carbonate with organic sulfonate anions. It is worth noting that even during filtering, washing and drying of modified anionic clays it is necessary to avoid carbonate contaminations. For this reason, after exchange, anionic clays are filtered in nitrogen atmosphere, washed with decarbonated water and dried in vacuo. For comparison the 3-aminobenzenesulfonate modified LDH was filtered and washed in three different ways; the clay MG61/ABS was filtered and washed in a nitrogen atmosphere as usual, MG61/ABSair was filtered and washed in air and MG61/ABSsx was washed in Argon with a Soxhlet extractor. In Fig. 4(a) the presence of a peak at 0.76 nm in the powder X-Ray diffraction of MG61/ABSair reveals that the adsorption of CO_2 from air is quick enough to cause—during filtration and washing—the formation of

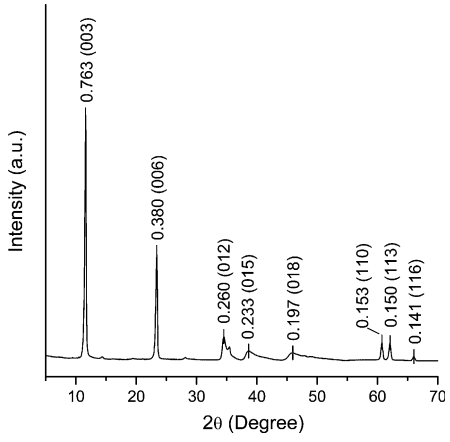

Fig. 2. Diffraction pattern of MG61 with its characteristic *d*-spacings and Miller indexing.

[6] According to ISO 31–8, the term 'molecular weight' has been replaced by 'relative molecular mass', symbol M_r. Thus, if this nomenclature and notation were used here, $M_{r,n}$ instead of the historically conventional M_w for the average molecular weight (with similar notation for M_w, M_z, M_v) would be used. It would be called the 'number average relative molecular mass'. The conventional notation, rather than ISO notation, has been employed here.

[7] The chemical formula of MG61 and its AEC are calculated using the data sheet supplied by the producer. In particular the AEC is calculated as follow: AEC $= x/M_w \times 10^5$ (mequiv/100 g), where M_w and x are the molecular weight and the layer charge per octahedral unit, respectively.

[8] From simple geometry and charge balance considerations, it is easy to show that $\sigma = 2x/(\sqrt{3}a2)$, where $a/2$ is the crystallographic (110) spacing.

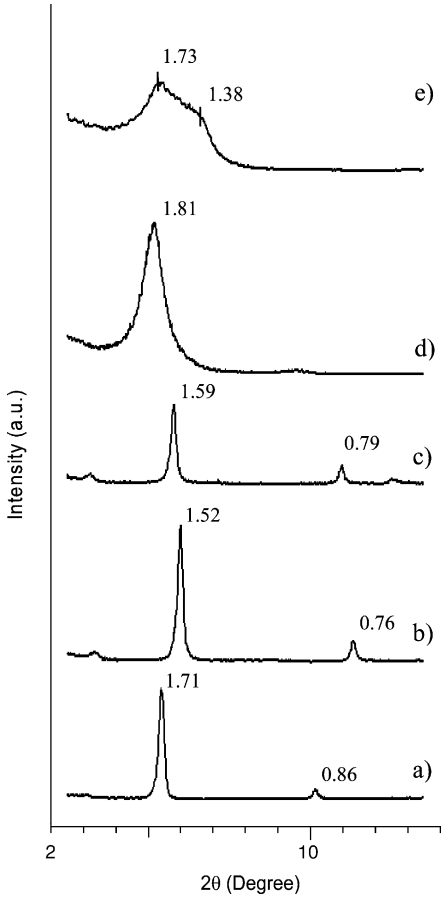

Fig. 3. Powder diffraction patterns of modified anionic and cationic clays: (a) MG61/TS, (b) MG61/HBS, (c) MG61/ABS, (d) 30B, (e) DelAP.

LDH carbonate. No peak related to a LDH carbonate was detected in MG61/ABS and MG61/ABSsx patterns (Fig. 4(b) and (c)). Furthermore MG61/ABSsx shows an increase of sharpness and intensity of XRD peak; this is

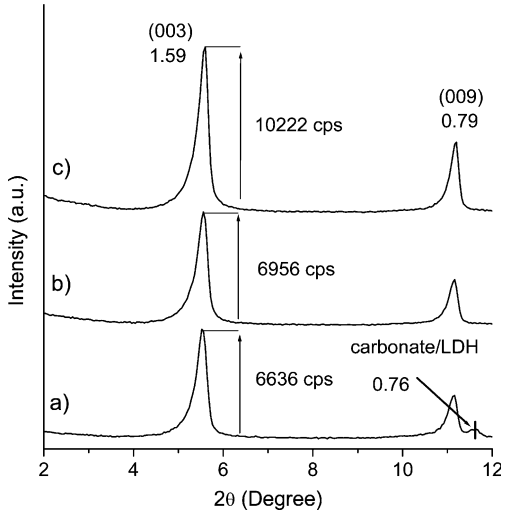

Fig. 4. Powder diffraction patterns of anionic clays modified with 3-aminobenzenesulfonate: (a) MG61/ABSair (air), (b) MG61/ABS (N_2 atmosphere), (c) MG61/ABSsx (Soxhlet extracted).

Table 3
Elemental analysis data of MG61/ABSsx

Element	[wt%]
Mg	11.61±0.76
Al	7.07±0.46
C	16.44±0.12
H	4.31±0.25
S	6.34±0.93
N	3.22±0.06
H_2O	7.01±0.19
Mole ratio	[mole/mole]
Mg:Al	1.82±0.15
S:Al	0.76±0.14
N:Al	0.88±0.03

Reported uncertainty is $\pm 2\sigma$, where σ is the standard deviation. The uncertainty of calculated ratios Mg:Al, S:Al and N:Al is obtained combining individual standard uncertainties according to the law of propagation of uncertainty.

considered to be proportional to the crystallinity [13,14]. It is reported that hydrothermal treatments increase the crystallinity and the particle size of LDH [15]. Thus Soxhlet extraction with water under reflux condition and inert atmosphere is a useful method for improving the crystallinity of organo-modified LDH.

MG61/ABSsx anionic clay was further characterized by elemental analysis; data are reported in Table 3. The molar ratio Mg:Al is decreased from ~2.0 in the pristine MG61 to ~1.8 in the organic-modified clay. The decrease of the Mg:Al ratio is not surprising. The LDH formation occurs trough a dissociation–deposition–diffusion mechanism [16]. The acid pH during exchange promotes the partial dissolution of the pristine LDH and the deposition of more acidic LDH with a higher Al content. It has to be mentioned that a small amount of amorphous $Al(OH)_3$, not detectable by XRD, can also be present in the product. This is supported by the solubility products pK_{sp} for $Mg(OH)_2$ and $Al(OH)_3$—respectively, 9.96 and 31.21 [17].

To guarantee the electro neutrality of LDH it is necessary that there is one intercalated monovalent anion for each Al atom. Instead, as reported in Table 3, both S:Al and N:Al ratios are less than 1[9]. Therefore, other anions, i.e. carbonate, are co-intercalated. This hypothesis is supported by the presence of the characteristic LDH carbonate peak at 788 cm^{-1} [18] in the FTIR absorption spectrum (Fig. 5). Peaks assigned at the presence of 3-aminobenzenesulfonate are also observed (S=O symmetrical stretching at 1031 cm^{-1}, CH aromatic in-plane bending at 1113 and 1170^{-1} cm). The carbonate LDH diffraction peak is not observed in the XRD pattern for MG61/ABSsx, whereas it is observed for MG61/ABSair (Fig. 4). This is the behavior

[9] In fact there is one S or N atom for each ABS anion. The small difference between S:Al and N:Al ratios may be related to adsorbed N_2 on the high surface area LDH. For this reason the S:Al ratio is preferred to estimate the number of intercalated ABS anions.

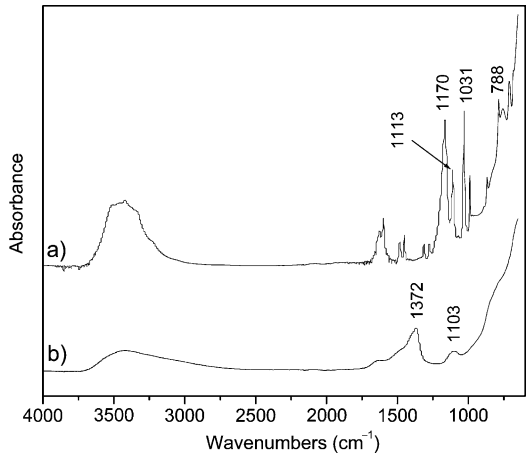

Fig. 5. FTIR spectra of: (a) MG61/ABSsx as synthesized; (b) MG61/ABSsx heated up to 900 °C in N_2 (ramp at 10 °C/min).

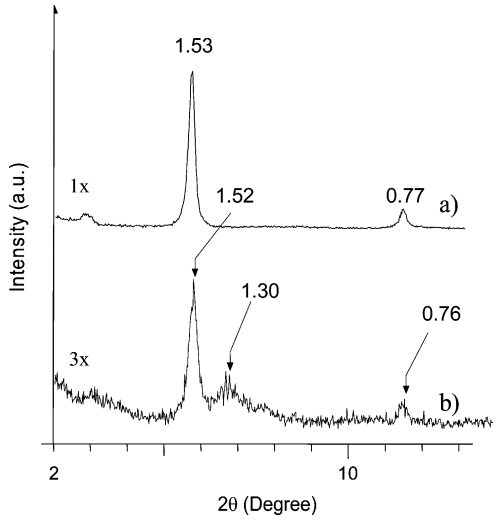

Fig. 7. XRD patterns of MG61/HBS: (a) Washed on the filter at 50 °C; (b) washed with hot water (90 °C).

expected for a layered solid with sufficiently rigid layers. A low amount of small carbonate anions are solubilized into the interlayer region of the large organic anions (e.g. ABS) without any detectable change in the *d*-spacing. Whereas, when the concentration of carbonate is too high as in MG61/ABSair, the segregation of carbonate phase occurs and the LDH carbonate can be detected by XRD [19]. On the basis of previous hypothesis and elemental analysis data, the nominal formula for octahedral unit of MG61/ABSsx is:

$$Mg_{0.65}Al_{0.35}(OH)_2(C_6H_4SO_3NH_2)_{0.27}(CO_3)_{0.04}\cdot 0.52H_2O \quad (2)$$

In Table 1 the experimental and theoretical *d*-spacing and the van der Waals dimensions of organic anions, calculated by means of computer modeling, are reported. The theoretical values of *d*-spacing are obtained assuming that anions are oriented with long axis perpendicular to brucite layers and that one water molecule is adsorbed on the hydroxyl layer. In general there is a good agreement between $d_{experimental}$ and $d_{calculated}$ in Table 1 except for MG61/HBS. For this modified LDH the possible anion arrangement in the gallery could be slightly tilted towards the layer. The relative low value of *d*-spacing in MG61/HBS could also be related to grafting reactions. In fact it is reported [20] that heating in mild conditions can activate grafting reactions by condensation between the OH group of the organic anion and the hydroxyl of the sheet (Fig. 6). These reactions were observed in Zn–Al and Cu–Cr LDH for aromatic carboxylates with OH groups substituted in *para* or *meta* positions, whereas no grafting was observed for amino, chloro or nitro substituted benzoate. These grafting reactions cause a contraction of *d*-spacing the extent of which depends on the position of the substituted group; maximum contractions (0.35–0.65 nm) are observed for *para* position. In Fig. 7 XRD patterns of MG61/HBS washed as usual on the filter at 50 °C and washed at 90 °C are shown. A 0.23 nm contraction of basal spacing, from 1.53 to 1.30 nm, was observed when the clay washing on filter was carried out with hot water (90 °C). Although further analyses are necessary to fully understand this behavior, this phenomenon may indicate that under mild conditions grafting reactions can be activated in MG61/HBS. We expect that grafting may create a structure between the LDH layers, which prevents exfoliation, due to the strong electrostatic interactions between hydroxyl layers and the sulfonate groups. This hypothesis is confirmed by the results of swelling (12 h 80 °C, 2 h 120 °C; 6.4 wt% clay) for the two epoxyphilic clays MG61/ABS (modified with amino substituted benzene sulfonate) and MG61/HBS (modified with hydroxy substituted benzene solfonate). In fact no intercalation was observed for MG61/HBS while a complete intercalation of epoxy monomer was observed for MG61/ABS. In this case the X-ray diffraction of the liquid sample (LXRD) shows four orders of basal reflections (Fig. 8), indicating that the intercalated structure is highly ordered. Similar results cannot be achieved with natural

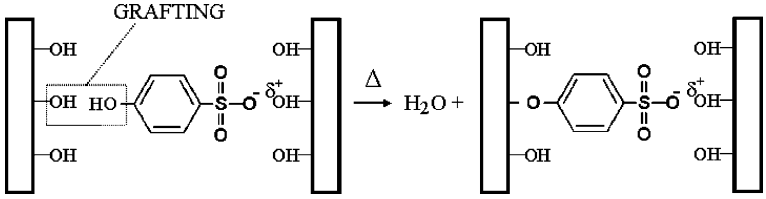

Fig. 6. Proposed scheme for grafting reaction by condensation between the OH group of hydroxybenzenesulfonate and the hydroxyl of the LDH.

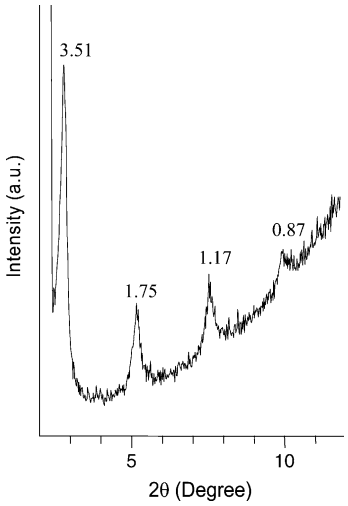

Fig. 8. Liquid X-ray diffraction pattern of the epoxy monomer with 6.4 wt% of MG61/ABS after swelling. The detected peaks are relative to the first four orders of basal reflections.

clays (e.g. layered silicates), due to impurities and variations in exchange capacity, which reduce the intensity of basal reflections. A thin layer of the same liquid epoxy sample, previously analyzed by LXRD and swelled with MG61/ABS, was spread on a grid and observed by TEM (Fig. 9(a)). The layers are clearly visible and the intercalated structure with a *d*-spacing of 3.51 nm detected by XRD is in agreement with TEM results. The same swelling was performed with MG61/ABSair, that (vide supra) is an

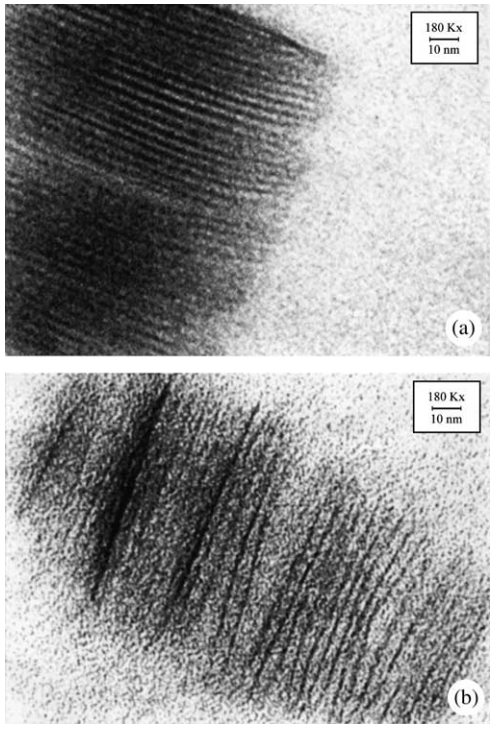

Fig. 9. TEM micrographs of: (a) Liquid epoxy monomer intercalated in MG61/ABS (6.4 wt%) after swelling; (b) same sample after curing with D230, ID name ABS-D230.

ABS modified LDH with impurities of LDH in the carbonate form. In this case LXRD (not shown) reveals the presence of the peak at 3.51 nm relative to the intercalate phase, and a residue peak at 0.76 nm related to the LDH in the carbonate form. Thus the presence of impurities of LDH in a carbonate form, avoids a complete swelling of the clay due to the high stacking force between hydroxyl layers and carbonate anions.

It is reasonable that, during the swelling process, the amino group of ABS modified LDH could react with oxirane rings of epoxy monomer. The reaction of one epoxy monomer with the amine groups of two facing lamellae (for the reminder bridging reaction), gives the formation of the structure depicted in Fig. 10, and prevents any further increase of the *d*-spacing. On the basis of computer modeling the van der Waals length of the epoxy monomer reacted with two ABS anion is 3.10 nm. Thus considering a lamella thickness of 0.48 nm [4] the calculated d spacing is 3.58 nm; it is in good agreement with the observed value of 3.51 nm (Fig. 8).

After swelling of clay the curing agent was added in a stoichiometric amount according to the procedure reported in Table 2 for each formulation. As shown in Fig. 1, the curing agents were primary diamine (DDS and D230) or tetramine (DEH). The X-ray diffraction patterns of samples containing anionic or cationic clays, and cured with D230, are reported in Fig. 11; in Fig. 12 the samples containing MG61/ABSsx cured with DDS and DEH are shown. For all the specimens, the peak related to the characteristic clay *d*-spacing it is not detectable and so it can be argued that a complete intercalation and/or delamination was obtained. In particular an intercalated structure was observed in TS-D230, 30B-230, ABSsx-DEH and ABSsx-DDS. No peak is observed for DAP-D230, but TEM micrograph (Fig. 13) shows an intercalated structure with an average *d*-spacing of about 7 nm; the large distribution of basal spacings may, in fact, cause the absence of (00l) reflections [21]. Similar results are observed for ABS-D230: In the TEM image (Fig. 9(b)) an intercalated structure with *d*-spacings between 3.7 and 17.0 nm is seen. It is proposed that the weak peaks of Fig. 11(a) are related to the second and third order of diffraction, respectively, this hypothesis allows an estimated *d*-spacing of about 5.6 nm. The importance of the organic modifier and, in particular, of its reactivity with epoxy monomer, is revealed by the different behaviour of cationic clays DelAP and 30B, and the anionic clays MG61/ABS and MG61/TS. DelAP and MG61/ABS are modified with reactive epoxyphilic groups: An acidic primary C(14–18) alkylmonoamine, and 3-aminobenzenesulfonate, respectively. The reactivity of ABS anions comes from the amine substitution in benzene sulfonate anions. The higher reactivity of primary alkylammonium compared to quaternary ones, comes from their acidity. Both reactive and unreactive compatibilizers are useful to preload the gallery region with epoxide monomer, but reactive compatibilizer can also catalyze the intragallery polymerization. Based on

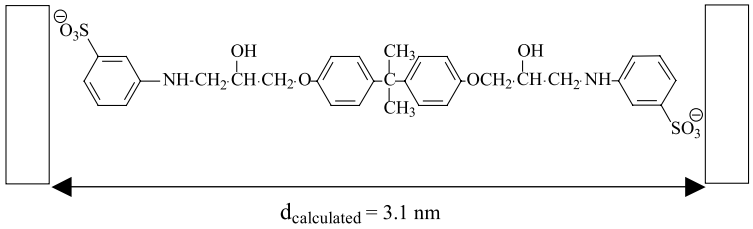

Fig. 10. Schematic model of the proposed bridged LDH obtained by reaction of oxirane rings of epoxy monomer with primary amine of ABS modified LDH.

the work by Lan et al. [7], the ratio between the intragallery and the extragallery polymerization rates must be tuned in order to exfoliate the clay in epoxy systems. Indeed, if this ratio is too slow, the polymerization rate outside the layers (extragallery polymerization) will be faster than the polymerization rate between the layers (intragallery polymerization) and only intercalated nanocomposites will form. In the present study, we observed that, independent of the nature of the clay, the *d*-spacing increases by using reactive compatibilizers. In fact, in the samples cured with D230, there is—for anionic clays—an increasing of *d*-spacing from 2.3 nm of TS-D230 to 5.6 nm of ABS-D230, while—for cationic clays—there is an increasing of *d*-spacing from 4.0 nm for 30B-D230 to 7.0 nm for DAP-D230.

To investigate the influence of the curing agent on the morphology of the nanocomposite the modified anionic clay MG61/ABS was used with three different hardeners: D230, DEH and DDS. Furthermore, *n*-butanol was used as a swelling agent for DEH and DDS cured systems. This approach was used because it was believed that the presence of a solvent in the interlayer region during swelling, could decrease the probability of bridging reactions between the epoxy monomer and ABS modified LDH. Actually the ABSsx-DEH and ABSsx-DDS showed a *d*-spacing after curing (3.3 and 3.4 nm, respectively) which was lower than the *d*-spacing observed after swelling (3.5 nm). The XRD data shown in Fig. 12 are confirmed by TEM micrographs (Figs. 14 and 15). According to Chen et al. [22], a *d*-spacing contraction of about 0.2 nm may be related to the stiffness of the extragallery polymer that, during curing, increases faster than the stiffness of the intragallery polymer such that the intragallery material becomes compressed. The different behavior of ABSsx-DEH and ABS-DDS compared to ABS-D230—where a sensible increase of basal distance was observed—could be explained by the different diffusion rate (i.e. polarity and mobility) and reactivity of the curing agents [7,21]. In fact, the low reactivity and high flexibility of aliphatic amine D230 allows a better diffusion in the intragallery region, compared to the rigid aromatic amine DDS, or the high reactive aliphatic tetra-amine DEH. Another possible explanation is related to the different swelling conditions used (Table 2): The higher temperature—during swelling and extraction of *n*-butanol—for DDS and DEH cured samples, compared to D230 cured samples, could promote bridging reactions in the interlayer region. Furthermore the presence of *n*-butanol during swelling of ABSsx-DEH and ABSsx-DDS increases the reactivity of oxyrane rings by a chain transfer mechanism

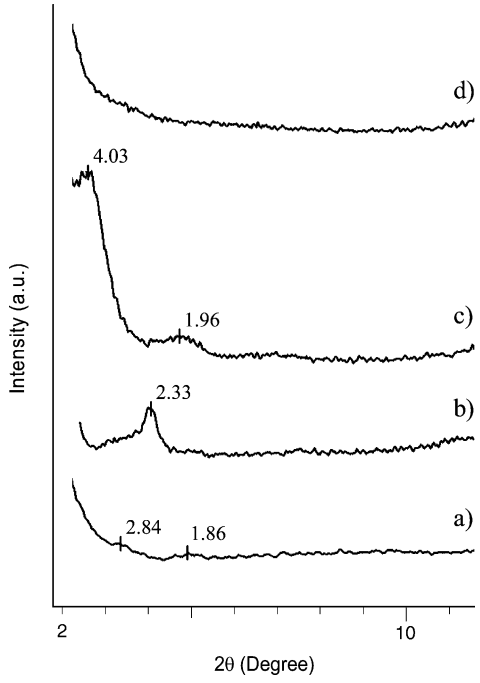

Fig. 11. X-ray diffraction patterns of the epoxy samples cured with D230 containing 5 wt% of modified clay: (a) ABS-D230; (b) TS-D230; (c) 30B-D230; (d) DAP-D230.

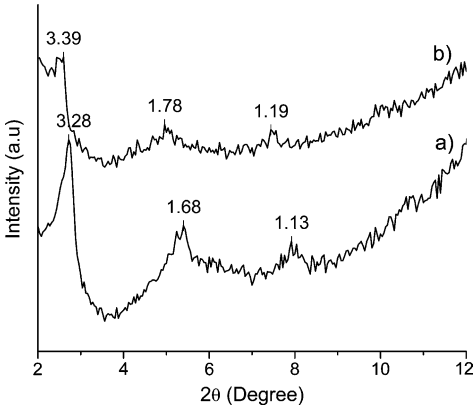

Fig. 12. X-ray diffraction patterns of the epoxy samples containing 5 wt% of MG61/ABSsx cured with: (a) DEH (sample ID:ABSsx-DEH); (b) DDS (sample ID:ABSsx-DDS).

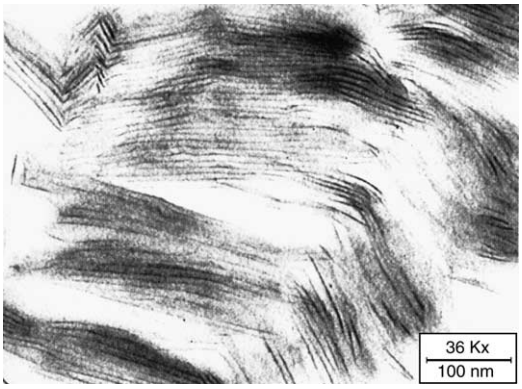

Fig. 13. TEM micrograph of: The epoxy nanocomposite containing 5 wt% of DelAP, cured with D230—ID name DAP-D230.

[23]. Thus it is reasonable to think that for ABS-D230 the bridging process is incomplete, whereas for ABSsx-DEH and ABSsx-DDS the numbers of bridging bonds is so high to prevent any further gallery expansion after swelling.

3.2. Thermal properties

As shown in Fig. 16 the decomposition mechanism of carbonate LDH-MG61—is a three step process. The first one, at low temperature, corresponds to the loss of interlayer water; this step is reversible [3,24]. The second and third steps at higher temperatures correspond to the condensation of hydroxyls of the octahedral layer, together with the decomposition of the anion CO_3^{2-}. The inorganic residue (~56.0 wt%) is composed by magnesium oxide and a spinel-like structure $MgAl_2O_4$. The decomposition of MG61 is strongly endothermic: The enthalpies of reactions are, respectively, 356 J/g for the first step, and 594 J/g for the second and third step. The heat absorption capacity of MG61 (950 J/g) is comparable with that of magnesium (1200 J/g) and aluminum hydroxides (1190 J/g).

After anionic exchange the organic modified clay presents two main steps of decomposition. The first one is related to the release of adsorbed and intercalated water, while in the second one the endothermic decomposition of hydroxyl layers is overlapped with the exothermic decomposition of organic anions. As an example the simultaneous thermal analysis (STA) for MG61/TS is reported in Fig. 17.

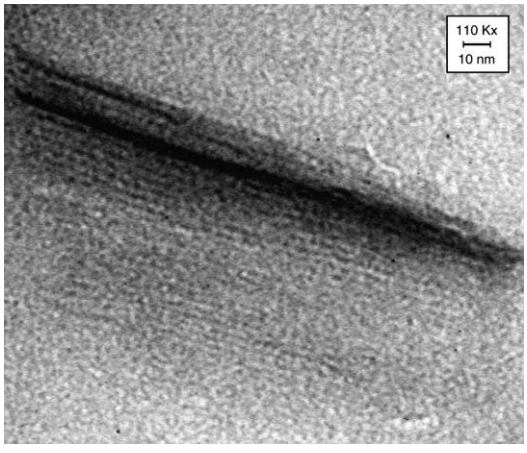

Fig. 14. TEM micrograph of the epoxy nanocomposite containing 5 wt% of MG61/ABSsx, cured with DDS—ID name ABSsx-DDS.

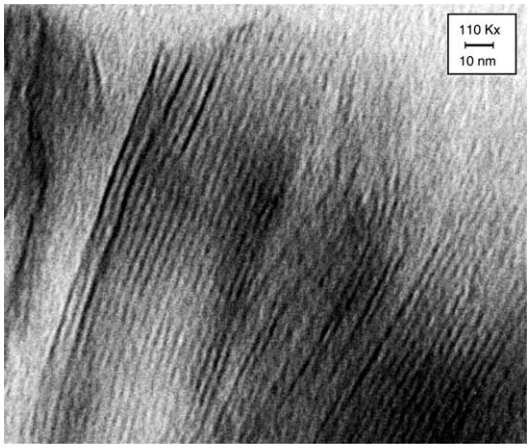

Fig. 15. TEM micrograph of the epoxy nanocomposite containing 5 wt% of MG61/ABSsx, cured with DEH—ID name ABSsx-DEH.

A similar pathway in the thermal decomposition of MG61/ABS was observed (Fig. 18). In this case the final residue at 900 °C was 40 wt%. From the Eq. (2) the theoretical inorganic residue (i.e. MgO and $MgAl_2O_4$) is only 37.6 wt%. It means that other species such as sulfate and/or organic moieties are still retained at 900 °C, as it was already reported for Zn–Cr LDH modified with 4-dodecylbenzenesulfonate [25]. This is further supported by FTIR absorption spectrum of the residue (Fig. 5); the peak detected at 1372 cm^{-1} is typical of $–SO_2–$ asymmetric stretching, likely due to $C–SO_2–C$ and/or $C–SO_2–N$ moieties, and the peak at 1103 cm^{-1} is characteristic of SO_4 asymmetric stretching [26].

The thermal degradation of epoxy resin in air is characterized by a double stage process: In the first stage, at about 370 °C, the main loss in weight occurs (~75%), while in the second stage, at 550 °C almost all the exothermicity is released, although the weight loss is only 25% for the second stage [27]. Such a trend is observed also in the nanocomposite sample filled with montmorillonite

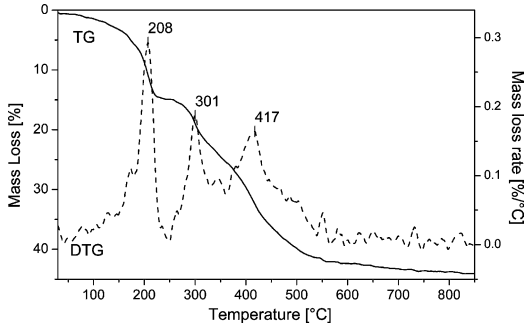

Fig. 16. Thermogravimetrical analysis of carbonate/LDH, ID name MG61.

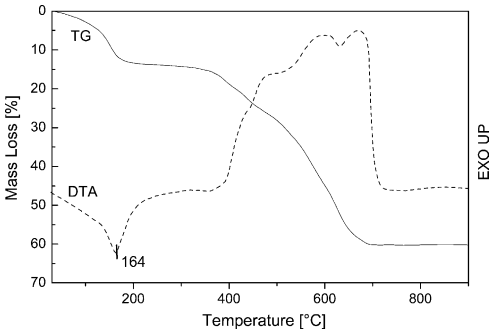

Fig. 17. Simultaneous thermal analysis of MG61/TS.

30B-D230 and the microcomposite filled with carbonate-LDH MG61-D230. However, TS-D230 epoxy nanocomposite has a different thermal degradation in air; the main exothermic peak is increased by more than 50 °C (Fig. 19).

In Figs. 20 and 21 the TGA of DDS and DEH cured samples are shown. In both cases the presence of MG61/ABS promotes char formation. The thermal stability of epoxy nanocomposites compared to the neat epoxy is unchanged for DEH cured samples, whereas a reduction of 18 °C in the onset of degradation temperature, is observed for the DDS cured samples. Char promotion and a decrease of thermal stability are observed in APP-DEH. The reduction of thermal stability in epoxy resins containing phosphorus has been reported in literature [28]. APP decomposes, at about 300 °C, into polyphosphoric acid and ammonia. The polyphosphoric acid catalyzes dehydration of the polymer [29], which is the first step of degradation of the epoxy network, and promotes the formation of unsaturated compounds with subsequent charring [30].

The charring agent precursor in intumescent systems is usually a phosphorous compound, in most cases APP, but sulphur compounds can also be used. Sulfonates (e.g. ABS anion) when heated decompose to form strong mineral acids which catalyze dehydration reactions [31]. For this reason we propose that MG61/ABS promotes charring reactions in epoxy nanocomposites. A further clue that charring is related to the nature of the surface modifier—rather than the LDH itself—comes from previous studies. Hsueh et al. [32]

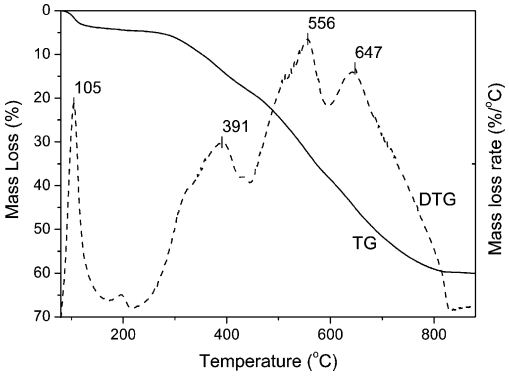

Fig. 18. Thermogravimetrical analysis of MG61/ABSsx.

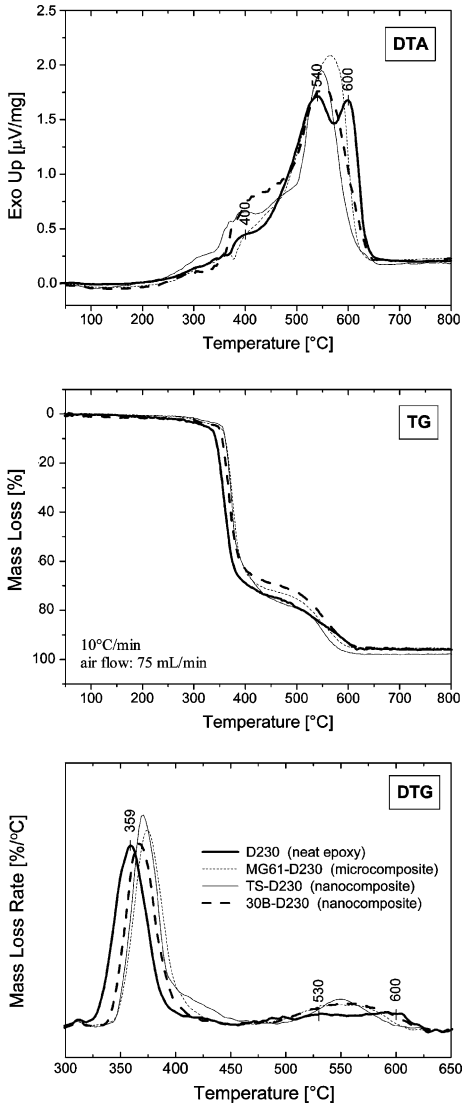

Fig. 19. Simultaneous thermal analysis in air of cured epoxies samples: (pure epoxy) D230, with LDH carbonate (microcomposite) MG61/D230, with organic modified LDH (nanocomposite) TS-D230, and with organic modified montmorillonite (nanocomposite) 30B-D230.

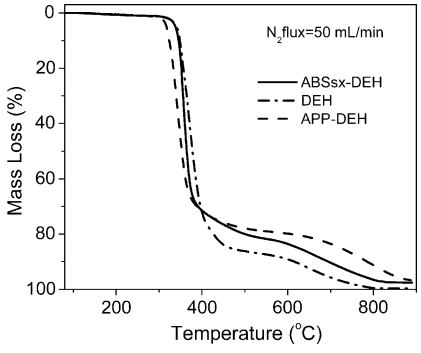

Fig. 20. Thermogravimetrical analysis of epoxy samples DEH, APP-DEH and ABSsx-DEH.

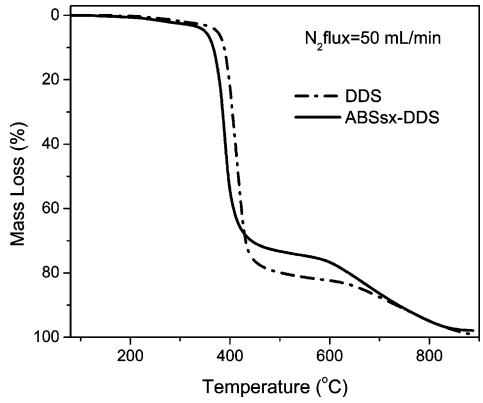

Fig. 21. Thermogravimetrical analysis of epoxy samples DDS and ABSsx-DDS.

prepared an epoxy nanocomposite based on LDH modified with an amino carboxylate (12-amino laurate), and they observed, compared to the pristine polymer, an increase of thermal stability due to the typical barrier effect of clays [33], but no increase of residue at higher temperature. On the other hand, Chen et al. [34], showed that in PE-*g*-MA nanocomposite based on a dodecyl sulphate modified LDH, the thermal stability is depressed, but charring of the polymer is enhanced. So it seems that the intercalated anion—and in particular its acidity—are the main factors which influence the degradation pathway by a charring mechanism.

3.3. Flame retardant properties

3.3.1. D230 cured samples

As deduced from UL 94 Horizontal Burning test [6], organic-modified LDH based nanocomposites—TS-D230 and ABS-D230—show higher flame-retardant properties compared to conventional nanocomposites based on organic modified montmorillonite (30B-D230 and DAP-D230) and to microcomposites containing traditional flame retardants, like ATH (ATH-D230) and MG61 (MG61-D230). In fact only LDH nanocomposites showed self-extinguishing behavior in the horizontal UL94 HB test; LDH micro-composites and montmorillonite based nanocomposites samples burned completely showing that the unique flame

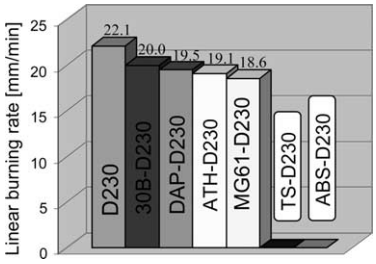

Fig. 22. Linear burning rates of epoxy samples obtained according UL94HB test; only LDH-epoxy nanocomposites, TS-D230 and ABS-D230, show self-extinguishing properties (the front flame did not reach the first mark at 2.5 cm or extinguished in the first 3 cm of the specimen).

resistance of LDH nanocomposites is related to both the level of dispersion and the intrinsic properties of the modified LDH (Fig. 22). To our knowledge these are the first examples of self-extinguishing nanocomposites which contains no other flame retardant used for the nano-additive.

Burning of the nano-dispersed LDH leads to the formation of an intercalated nanostructure of mixed metal oxides (produced by thermal degradation of LDH) and char. This hypothesis is supported by XRD, due to the presence of a peak at 1.28 nm in the TS-D230 and ABS-D230 nanocomposite after UL 94 test (Fig. 23(d)). Gilman et al. reported an intercalated structure of char from montmorillonite nanocomposites, with the same interlayer spacing of the chars, 1.3 nm, independent of the chemical structure of the polymer (thermoplastic or thermosetting) or nanostructure (delaminated or intercalated) [33]. The same value observed in LDH based nanocomposite (1.28 nm) shows that the interlayer spacing of char may be independent of the nature of the layered crystal.

Cone calorimeter analyses confirm the higher performance of LDH nanocomposites compared to montmorillonite nanocomposites (Table 4). ABS-D230 and TS-D230 show a reduction of the peak of heat release rate (PHRR) of 51 and 40%, respectively, compared with the neat epoxy resin. This result is much better that the one achieved with montmorillonite DAP-D230 (27% reduction of PHRR). The slow heat release of ABS-D230 and TS-D230 can be justified by the formation of a compact residue with an intumescent behaviour, whereas the surface of DAP-D230, after cone calorimeter test, is completely fragmented (Fig. 24). The ABS-D230 residue, after cone calorimeter test, shows a thin shell structure. The thickness of this shielding layer is about

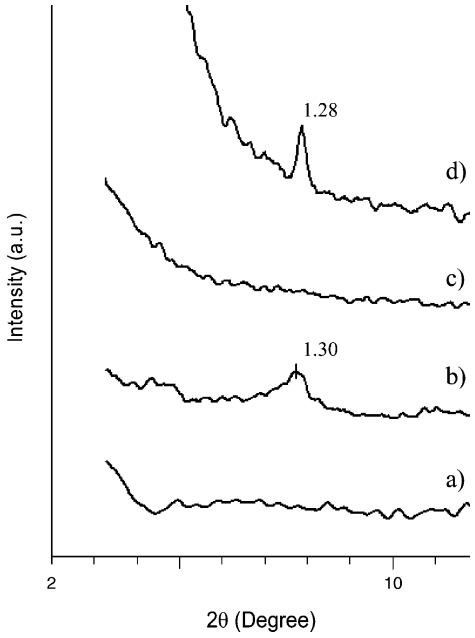

Fig. 23. X-ray diffraction patterns of char of: (a) D230 after UL94 HB; (b) DAP-D230 after cone calorimeter; (c) TS-D230 after cone calorimeter; (d) TS-D230 after UL94HB.

Table 4
Cone calorimeter data

Sample ID	Residue yield (%)	Peak HRR (kW/m^2) (Δ%)	Mean HRR (kW/m^2) (Δ%)	Mean H_c (MJ/kg)	Mean MLR (g/s m^2)	Mean SEA (m^2/kg)	Ignition time (s)
D230	3.3	1181	533	26	23	750	109
DAP-D230	8.6	862 (27)	477 (11)	23	21	773	110
TS-D230	8.4	715 (40)	382 (28)	23	17	724	98
ABS-D230	9.5	584 (51)	347 (35)	22	15	743	112
APP-D230	90.1	491 (62)	105 (80)	17	6	720	78
DEH	4.6	1007	612	26	24	1082	144
DEH (*)	5.1	2576	1060	29	39	753	105
ABSsx-DEH	11.3	812 (19)	528 (14)	26	21	1013	130
ABSsx-DEH (*)	9.9	1422 (45)	821 (23)	27	33	632	95
APP-DEH	86	208 (79)	131 (79)	18	7	411	120
APP-DEH (*)	21.0	985 (62)	522 (51)	17	32	691	84
DDS	11.2	685	447	24	19	985	170
DDS (*)	9.5	1954	873	26	35	633	111
ABSsx-DDS	20.5	504 (26)	329 (26)	25	13	1171	109
ABSsx_DDS (*)	17.5	1210 (38)	658 (25)	25	26	786	90

Heat Flux, 35 kW/m^2. H_c, specific heat of combustion; SEA, specific extinction area. Peak heat release rate, mass loss rate, and SEA data are reproducible to within ±10%. The heat of combustion and the time to ignition data are reproducible to within ±15%. The thickness is 3 mm for samples with (*) and 8 mm for the others.

1 mm and it reaches a maximum height of 5 cm. This structure is brittle, but has good mechanical strength, integrity, coherence and adherence to the substrate. As shown in Fig. 25, the shell has a bi-layer structure: The internal face, white and porous, is formed by metal oxides, whereas the external face, black and compact, is formed by carbonaceous residues (some of which may be from soot formed in the gas phase).

LDH based nanocomposites, after UL94 HB, presented an intercalated structure of the residue with an interlayer spacing of 1.28 nm (vide supra), whereas, after cone calorimeter, no peak could be detected by XRD (Fig. 23). Actually cone calorimeter and UL94 HB present different testing conditions. In UL94 the flame on the sample is the only source of heat so after the extinguishing of flame the char is not subjected to oxidation. Instead in the cone calorimeter the residue is exposed to an external heat flux during burning and after flame extinction until it is removed from the device (~2 min). After the flame extinction, LDH based nanocomposites show a strong incandescent afterglow which forces the residual carbon to be at least partially oxidized to CO and CO_2. This is due to the products of decomposition of LDH—magnesium/aluminum oxides—that catalyze oxidation reactions to produce afterglowing [35–37]. Therefore, we propose that during combustion of the LDH based nanocomposites, first, an intercalated structure char/metal oxides is formed and, then, during afterglowing, the intercalated carbonaceous residue is oxidized to CO and CO_2 by a reaction that is catalyzed by the metal oxides themselves.

The comparison between the heat release rate of epoxy samples cured with D230 is reported in Fig. 26. It is worth noting that the strong reduction of heat release observed in TS-D230 and ABS-D230 after about 160 s, it is coincident with the rapid expansion of char. Thus LDHs modified with organic sulfonates (i.e. MG61/ABS and MG61/TS) act as a nano-intumescent system, where the epoxy resin itself is the source of the char, the sulfonate is the charring agent (vide supra), while water and CO_2 (evolved during the thermal decomposition of hydroxyl layers) are the blowing agents. The organic modifier can also act as blowing agent and, in fact, the higher swelling, displayed by MG61/ABS compared to MG61/TS, is likely due to the evolution of ammonia produced by the thermal degradation of ABS.

In terms of weight loss and heat release, nanocomposites are less effective compared with APP-D230 but, on the other hand, APP reduces thermal stability and hence, the ignition time by 29%. ABS-D230 and TS-D230 show a comparable ignition time with that of neat resin. Furthermore, APP causes a depletion of mechanical properties of epoxy, whereas LDH based epoxy nanocomposites show an increase of tensile strength, Young's modulus, strain at break and a reduction of thermal expansion and permeability [32,38].

Most importantly, even if the effectiveness of MG61/ABS alone is lower than the one of APP, MG61/ABS shows a synergistic effect with APP. In fact, in order to comply with the UL94-V0 standard, for 3 mm thick samples, a 30 wt% adding of APP was necessary in D230 cured epoxy, whereas using a 4 wt% MG61/ABS, the APP content necessary was 16–20 wt%. It is reasonable to think that by decreasing the content of APP the mechanical properties of the formulation are increased. Similar synergistic effects were already observed for montmorillonite-APP-pentaerythritol (PER) systems in polypropylene [39]; Bourbigot et al. [40] showed that, in ethylene vinyl acetate (EVA) formulations, the use of PA-6 with montmorillonite (2 wt%) not only allowed removal of as much as one-third of the APP while a V-0 rating was maintained, but also an increase in elongation at break from 800 to 850%. Gilman et al. [41] found a seemingly

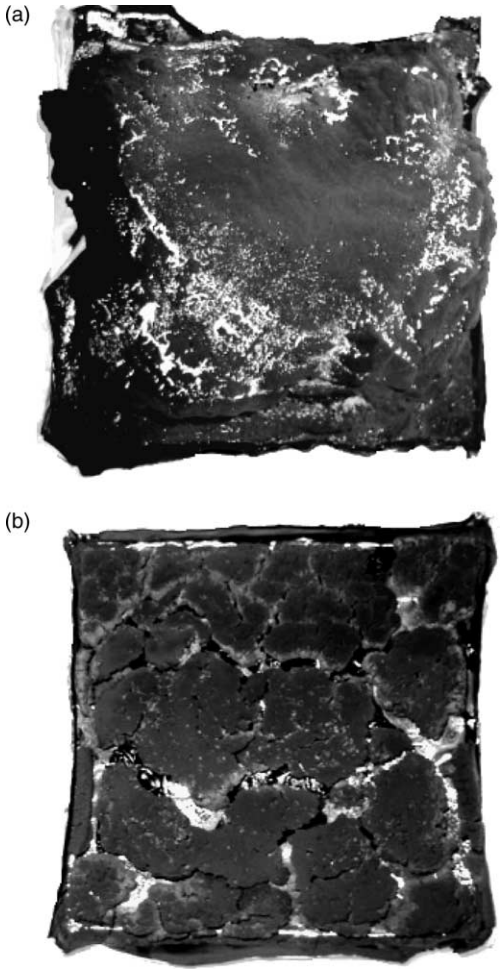

Fig. 24. Comparison of carbonaceous residue obtained after cone calorimeter tests: (a) Compact char of ABS-D230 (LDH-nanocomposite) with an intumescent behaviour (char thickness up to 5 cm); (b) fragmented char of DAP-D230 (montmorillonite-nanocomposite).

contradictory set of results in polystyrene. At low loading APP/PER (up to 20%) combined with 2% loading of organo-clay produces an increase of MFFS (minimum flux for flame spread) in excess of what would be obtained simply by adding additional APP/PER. Whereas, in the formulations with higher loading of both flame retardants the combinations produces a decrease in MFFS. These results suggest that the interactions between APP and clays are not fully understood. This is particularly true for nanocomposites material based on LDH, where the endothermic decomposition of the inorganic layers and the charring effect of the surfactant may play an important role.

3.3.2. DDS and DEH cured samples

As reported in Table 4, the LDH based nanocomposites cured with DDS and DEH also show a reduction of peak of heat release rate. However, in this case the reduction is lower than for D230 cured samples, and the combustion is accompanied with less intumescent effect. This behaviour could be due to a higher crosslinking density which increases

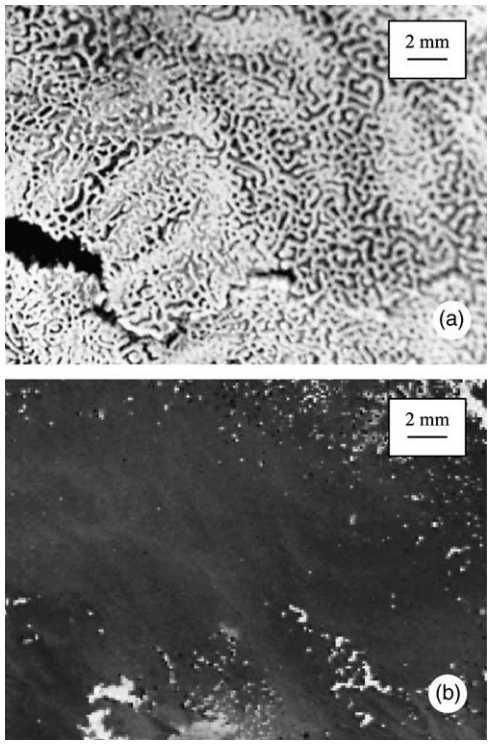

Fig. 25. Residue of ABS-D230 after cone calorimeter test: (a) White porous structure of mixed oxides on the internal face; (b) black compact carbonaceous residue on the external face.

the viscosity of polymer during charring and prevents swelling [42]. In this case the time to ignition is decreased in comparison to the neat polymer. As described before, the presence of *n*-butanol during swelling of ABSsx-DEH and ABSsx-DDS can plasticize the epoxy resin by a chain transfer mechanism. It is believed that plasticization, or a residue of intercalated butanol, decrease the time to ignition of the nanocomposite. The comparison between epoxy samples cured with DDS and DEH is reported in Figs. 27 and 28.

The effect of sample thickness on the heat release was studied with two different sample thicknesses of 3 and 8 mm. The ignition occurred much earlier and heat release

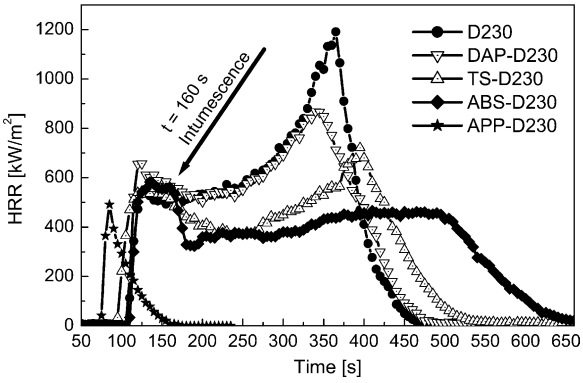

Fig. 26. Cone calorimeter curves of D230 cured samples. The intumescent behaviour of LDH based nanocomposites, TS-D230 and ABS-D230, starts at about $t = 160$ s.

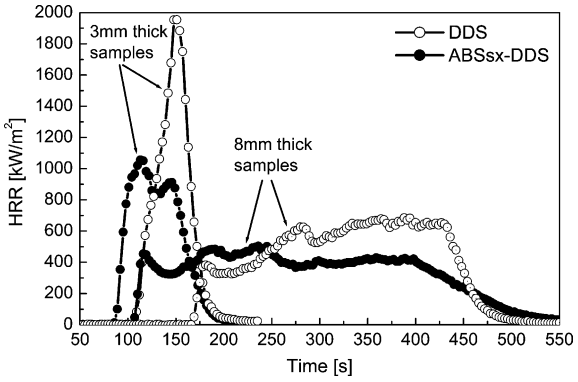

Fig. 27. Cone calorimeter curves of DDS cured samples.

rate increased more rapidly for the thinner sample than for the thicker sample. The flame retardant performance of the LDH nanocomposites is significantly increased for the thin samples compared to the thick samples. As reported in Table 4, ABSsx-DDS and ABSsx-DEH nanocomposites show, in comparison to the neat epoxy, a decrease in the PHRR, respectively, of 38 and 45% for 3 mm thick samples, and a decrease of PHRR of 26 and 19% for 8 mm thick samples. Gilman et al. [43] reported for polyamide 6/montmorillonite (5 wt%) nanocomposites that the trend in function of sample thickness was opposite. The reduction of PHRR, in comparison with the neat polymer, was about 60% for the 8 mm thick samples and 20% for the 1.6 mm thick samples. This is the usual result seen in charring systems [43]. In LDH based epoxy nanocomposites, due to the complexity of flame retardant mechanism, which involves swelling, barrier and charring effect, further investigations must be performed to fully understand the influence of sample thickness. The superior performance of thin samples LDH nanocomposites indicates they may have excellent potential for thin walled FR products.

4. Conclusions

Organo-modified anionic clays were prepared by ionic exchange in an acid medium with a synthetic magnesium–aluminum carbonate LDH precursor. The influence of synthesis conditions during anionic exchange, filtering, washing and drying were studied; it was shown that Soxhlet extraction is a valid system to obtain highly crystalline organic-modified LDH with low carbonate contamination. The use of reactive surfactant increased the compatibility between epoxy and LDH. Swelling conditions (e.g. temperature, swelling agents) influence the final *d*-spacing observed in the nanocomposite in particular for LDH modified with reactive compatibilizer, due to bridging reactions. The use of precursors of strong mineral acids (i.e. sulfonate anions) as modifiers, catalyze charring reactions in LDH based nanocomposites during thermal degradation, enhancing the formation of a carbonaceous char and decreasing the release rate of combustible volatiles.

Concerning the flame retardant properties, epoxy nanocomposites based on the organic-modified layered double hydroxide exhibit:

- A unique self-extinguishing behaviour in UL94HB test, never observed before in a pure nanocomposite.
- A higher reduction in the PHRR (peak of heat release rate) compared to montmorillonite based nanocomposites.
- An increase in the reduction of PHHR for the thin sample compared to the thick sample.
- The formation of an intumescent compact char with an intercalated nanostructure.
- A synergistic effect with ammonium polyphosphate.

In conclusion it is shown that LDH based nanocomposites may be used for the preparation of halogen-free and environmental-friendly flame retardant epoxy formulations.

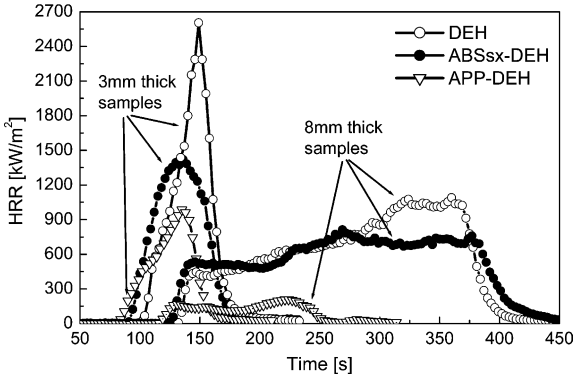

Fig. 28. Cone calorimeter curves of DEH cured samples.

Acknowledgements

The authors gratefully thank Dr Monica Celotto and Richard Harris for their contribution, and Dr Alexander Malyschew and Olaf Torno (Sasol Germany GmbH) for helpful discussions and for providing synthetic LDH carbonate. We are indebted to Cinzia Della Porta (Laviosa Chimica Mineraria) for her skilful assistance in montmorillonite modifications. Mauro Zammarano thanks NIST and CimtecLab for providing travel funds to support a guest research position at NIST. Jeff Gilman thanks William Hora for inspirational discussions.

References

[1] Cavani F, Trifiro' F, Vaccari A. Catal Today 1991;11:197.
[2] Leroux F, Besse JP. Chem Mater 2001;13:3507.
[3] Camino G, Maffezzoli A, Braglia M, De Lazzaro M, Zammarano M. Polym Degrad Stab 2001;74:457.
[4] Meyn M, Beneke K, Lagaly G. Inorg Chem 1990;29:5201.
[5] Cone Calorimeter Test, ASTM E 1354/1992.

[6] Ul94-Test for flammability of plastic materials for parts in devices and appliances, Underwrites Laboratories Inc.; 1997.
[7] Lan T, Kadiratna PD, Pinnavaia TJ. Chem Mater 1995;7:2144.
[8] Jacobson AJ. Mater Sci Forum 1994;152:1.
[9] Hibino T, Jones WJ. Mater Chem 2001;11:1321.
[10] Vaccari A. Catal Today 1998;53.
[11] Chatelet L, Bottero JY, Yvon J, Bouchelaghem A. Colloids Surf, A 1996;111:167.
[12] Doeuff M, Kwon T, Pinnavaia T. Synth Met 1989;34:609.
[13] Mohmel S, Kurzawski I, Uecker D, Muller D, Muller D, Gebner W. Cryst Res Technol 2002;37:4.
[14] Kannan S, Jasra RV. J Mater Chem 2000;10:2311–4.
[15] Oh JM, Hwang SH, Choy JH. Solid State Ionics 2002;151:285–91.
[16] Xu ZP, Lu GO. Chem Mater 2005;17:1055–62.
[17] Boclair JW, Braterman PS. Chem Mater 1999;11:298–302.
[18] Xu ZP, Braterman PS. J Mater Chem 2003;13:268–73.
[19] Constantino U, Coletti N, Nocchetti M. Langmuir 2000;16:10351–8.
[20] Prevot V, Forano C, Besse JP. Appl Clay Sci 2001;18:3–15.
[21] Kornman X, Lindbergb H, Berglunda LA. Polymer 2001;42:4493–9.
[22] Chen JS, Poliks MD, Ober CK, Zhang Y, Wiesner U, Giannelis E. Polymer 2002;43:4895–904.
[23] Hartwig A, Schneider B, Luhring A. Polymer 2002;43:4243–50.
[24] Bellotto M, Rebours B, Clause O, Lynch J. J Phys Chem 1996;100: 8535–42.
[25] Crepaldi EL, Pavan PC, Tronto J, Valim JB. J Colloid Interface Sci 2002;248:429–42.
[26] Colthup NB, Daly LH, Wiberley SE. Introduction to infrared and Raman spectroscopy. 3rd ed. New York: Academic Press; 1990.
[27] Kotsilkova R, Petkova V, Pelovski Y. J Therm Anal Calorim 2001;64: 591–8.
[28] Wu CS, Liu YL, Chiu YS. Polymer 2002;43:4277–84.
[29] Clariant GmbH. Polym Degrad Stab 1999;64:427–31.
[30] Levchik SV, Camino G, Costa L, Luda MP. Polym Degrad Stab 1996; 54:317–22.
[31] Rhodes PR. Fourteenth annual BCC conference on flame retardancy 2003.
[32] Hsueh HB, Chen CY. Polymer 2003;44:5275–83.
[33] Gilman JW, Kashiwagi T, Nyden M, Brown JET, Jackson CL, Lomakin S, et al. Chemistry and technology of polymer additives. Oxford, UK: Blackwell Science; 1999, chapter 14.
[34] Chen W, Qu B. Chem Mater 2003;15:3208–13.
[35] Delfosse L, Baillet C. Polym Degrad Stab 1998;23:337–47.
[36] Hull RT, Wills CL, Artingstall T, Price D, Milnes GJ. Fire retardant mechanism relating to smoke and toxic products yield from EVA composites, oral presentation. Recent advances in flame retardancy of polymeric materials, Stamford, Connecticut 2003.
[37] Rychly J, Vesely K, Gal E, Kummer M, Jancar J, Rychla L. Polym Degrad Stab 1990;30:57–72.
[38] Gensler R, Groppel P, Muhrer V, Muller N. Part Syst Char 2002;19: 293–9.
[39] Tang Y, Hu Y, Wang S, Gui Z, Chen Z, Fan W. Polym Int 2003;52: 1396–400.
[40] Bourbigot S, Le Bras M, Dabrowski F, Gilman JW, Kashiwagi T. Fire Mater 2000;24:201.
[41] Gilman JW, Davis RD, Shields JR, Harris RH. J Testing Evaluation, in press.
[42] Longdon P, Dowling J. Off-site fire protection: Developments in technology. Ninth European meeting on fire retardancy and protection of materials proceedings, Lille, 2003.
[43] Gilman JW, Bourbigot S, Shields JR, Nyden M, Kashiwagi T, Davis RD, et al. Mater Sci 2003;38:4451.